Thermoresponsive Host Polymer Matrix for Self-Healing Luminescent Solar Concentrators

Elisavet Tatsi,[†] Giovanni Fortunato,[†] Benedetta Rigatelli,[†] Guanpeng Lyu,[‡] Stefano Turri,[†] Rachel C. Evans,[‡] and Gianmarco Griffini*,[†]

[†]Department of Chemistry, Materials and Chemical Engineering "Giulio Natta", Politecnico di Milano, Piazza Leonardo da Vinci 32, 20133 Milano, Italy

[‡]Department of Materials Science & Metallurgy, University of Cambridge, 27 Charles Babbage Road, Cambridge CB3 0FS, U.K.

Ⓢ Supporting Information

ABSTRACT: Luminescent solar concentrators (LSCs) are a promising solar energy technology for reducing architectural barriers to the integration of photovoltaic systems into the built environment. In this work, the first demonstration of thin-film LSCs based on a thermally reversible cross-linked host polymer is presented. This smart material is obtained via a dynamic-chemistry approach based on the Diels−Alder (DA) reaction between a furan-functionalized acrylic copolymer and an aliphatic bismaleimide to obtain optically clear, cross-linked systems capable of healing mechanical damage upon heat treatment. By carefully tuning the concentration of a perylene-based luminophore dopant, an optical efficiency as high as 4.9% can be achieved with this DA-based LSC. In addition, full recovery of device efficiency is demonstrated after complete thermal healing of mechanically induced surface damages as a result of the embedded DA functionality. The approach presented here paves the way to the development of highly efficient multifunctional thermoresponsive smart LSC systems.

KEYWORDS: luminescent solar concentrators, self-healing polymers, Diels−Alder, stimuli-responsive polymers, photovoltaics, coatings
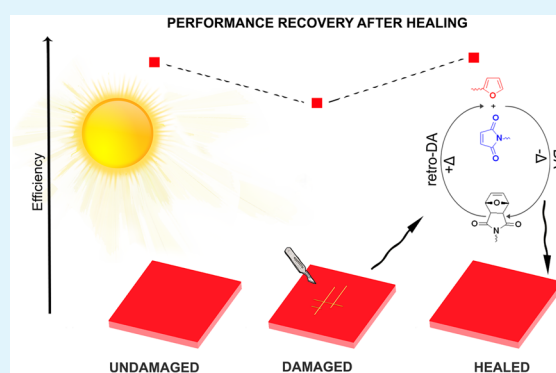
INTRODUCTION

Luminescent solar concentrators (LSCs) are a practical approach to potentially convert the facades of urban buildings into semitransparent electricity-generating elements. Their light weight, easy tunability in shape and color, ability to work well also under diffuse light, and to concentrate sunlight without the need of cooling or tracking equipment make them suitable candidates for seamless application in the building-integrated photovoltaics (BIPV) field.[1−3]

In its basic design, a LSC consists of a transparent host material (in the form of a bulk slab or a thin coating film deposited onto a transparent substrate) doped with one or more luminescent species (i.e., luminophores) serving the function of collector and spectral converter of incident light. Photons absorbed by these luminophores are re-emitted at longer wavelength (usually by fluorescence), and a portion of the downshifted light is trapped within the host matrix and waveguided toward the edges of the LSC device where it becomes concentrated. Collection of the concentrated light is undertaken by small-area PV cells that are responsible for the conversion of the optical power exiting the LSC edges into electrical energy.

The optical performance of an LSC is determined by the interplay between different loss pathways taking place in the system during the processes of photon absorption, re-emission, and transport, which can be directly related to either the luminophore or the host waveguide.[4] In particular, light-harvesting efficiency, photoluminescence quantum yield (PLQY), and self-absorption are directly associated with the optical properties of the selected luminophore. On the other hand, the light-trapping efficiency, surface reflections, parasitic absorption, and scattering losses are intimately linked to the nature of the host waveguide material. To tackle such loss mechanisms and enhance LSC optical efficiency, previous research has largely focused on the development of novel luminescent species to ensure broad light collection, effective photon emission, and limited absorption−emission spectral overlap. Among these, the most popular are organic dyes, inorganic quantum dots, and metal complexes.[1,5−9]

Compared to luminophores, host waveguide materials have been less intensely investigated, despite the fundamental role they play in the basic working principles and ultimate efficiency of LSCs. In particular, photon harvesting and transport processes are greatly affected by reflection and scattering
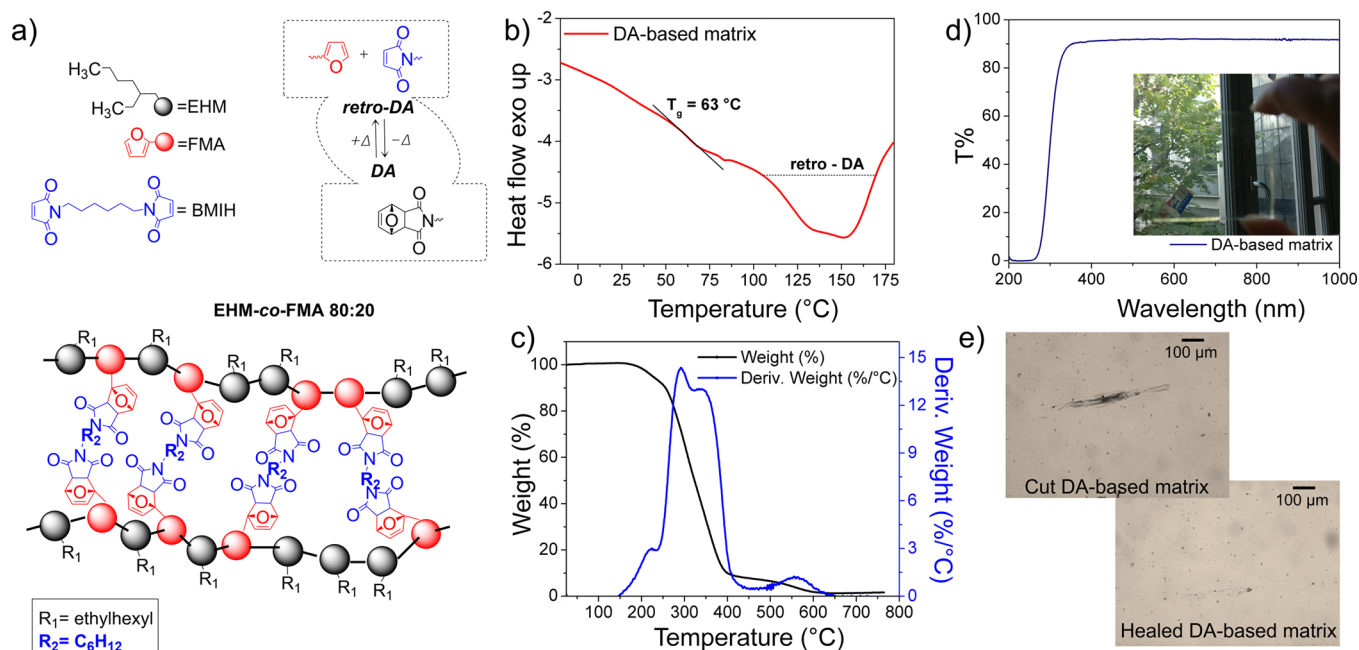
Figure 1. (a) Schematic representation of the chemical structure and functionality of the DA matrix presented in this work. (b) DSC plot of the cross-linked DA matrix. (c) TGA/dTGA plots of the DA matrix performed in air. (d) Transmittance spectrum of DA-based matrix. Inset: photographic image of a glass substrate coated with the DA matrix. (e) Optical microscope images of the DA-based matrix after being cut with a lancet and after thermally induced healing.

losses due to surface imperfections of the waveguide and by parasitic absorption resulting from its poor optical clarity. Similarly, the PLQY of the luminophore is typically dependent on its solubility in the host matrix, which is therefore critical for efficient absorption and emission processes.

Traditionally, glass or optically clear plastics such as poly(methyl methacrylate) (PMMA) or polycarbonate (PC) have been considered as viable host waveguides in LSCs due to their relatively low cost, high transparency, and suitable refractive index.[12,13] In recent years, the quest for high performance host waveguides has led to the development of novel alternative material concepts with enhanced chemical, physical, and optical characteristics.[14] Within this context, a variety of systems have been introduced, including bio-based polymers,[14−17] vacuum-deposited polymers,[18,19] fluorinated polymers,[20−22] and ureasil-based organic−inorganic hybrids,[23−26] each providing specific functions to the final LSC device. While the application of such host waveguide systems has yielded significant progress in terms of LSC design architecture,[27−32] matrix−fluorophore interactions,[33−37] and device performance,[12,38,39] some critical issues associated with the host waveguide component still remain.[40]

In particular, an important aspect still open in the field is the physical durability of LSCs and its effect on performance retention in real-life working conditions. In this context, physical damages potentially occurring to the surface of the LSC waveguide due to mechanical interaction with harsh weather phenomena, dust, or solid particles may reduce its surface smoothness, thus increasing the scattering of photons during transport caused by the presence of imperfections and optical defects at the waveguide/air interface. A measurable decay of LSC performance is to be expected in these conditions as a result of the reduced photon trapping efficiency of the waveguide.[41−44] Strategies to recover such surface

damages should therefore be sought to ensure prolonged device lifetime and sustained efficiency.

Within this framework, the first demonstration of a smart LSC system based on a stimulus-responsive polymer with thermoreversible cross-linking behavior is presented in this work. This system was obtained by exploiting a dynamic-chemistry approach based on the Diels−Alder (DA) reaction[45] between a new furan-functionalized acrylic copolymer and an aliphatic bismaleimide to obtain highly transparent thermoreversible cross-linked materials with excellent thermally induced healing capabilities. Thin films of DA polymers embedding a perylene-based fluorophore at increasing concentrations were deposited on glass substrates, and their optical, functional, and device properties as stimulus-responsive LSCs were investigated. To test the healing capability of such new DA-based LSCs, surface damages were mechanically induced on the doped waveguide, leading to a noticeable decrease in device efficiency. After a suitable thermal treatment, full recovery of the surface damage and of device efficiency was observed thanks to the built-in DA functionality.

■ RESULTS AND DISCUSSION

The novel stimulus-responsive polymeric network was obtained by equimolar reaction between a bifunctional linear aliphatic maleimide cross-linker (1,6-bismaleimidohexane, BMIH) and an acrylic-based copolymer bearing furan functional groups as lateral moieties (ethylhexyl methacrylate-co-furfuryl methacrylate, EHM-co-FMA, molar ratio 80:20). As schematically depicted in Figure 1a, BMIH serves as a reversible cross-linking bridge between EHM-co-FMA macromolecular chains and takes part in the DA cycloaddition reaction occurring between the maleimide (dienophile) group in BMIH and the furan (diene) moiety in EHM-co-FMA.

To confirm successful cross-linking and formation of the DA adduct, Fourier-transform infrared (FTIR) spectroscopy analyses were performed on as-cast and on thermally treated (150 °C for 20 min, followed by slow cooling to ambient temperature) coatings (Figure S1, Supporting Information). The disappearance of signals assigned to C=C (845 cm^{-1}), C−H out-of-plane bending (699 cm^{-1}), and =C−H (3110−3090 cm^{-1}) groups characteristic of BMIH upon thermally treating the coating material clearly demonstrated the occurrence of the DA reaction and formation of the corresponding DA adduct.[46] Direct evidence of the cross-linked nature of the coating was provided by gel-content measurements performed by immersing the thermally treated material into tetrahydrofuran (THF, a good solvent for both BMIH and EHM-co-FMA) for 24 h. The residual gel content was found to be over 99% with no noticeable weight loss in the material, proving the effectiveness of the curing process and the excellent chemical resistance of the coating system (Figure S2).

To verify the suitability of our cross-linked DA polymeric system as a host matrix for LSCs, its thermal, optical, and functional characteristics were evaluated. Differential scanning calorimetry (DSC) revealed a single glass-transition temperature (T_g) (Figure 1b), indicating the absence of phase segregation in the material as a result of the mutual compatibility and successful reaction between EHM-co-FMA and BMIH. More importantly, the observed T_g value (63 °C) is compatible with the typical service temperatures experienced in urban environments (40−50 °C, depending on the geographical location),[47] confirming the applicability of this material for outdoor LSC purposes. From the DSC trace, another important endothermic signal at 150−160 °C was clearly visible, which can be associated with the retro-DA process. When the coating is heated above its retro-DA temperature (the onset of the endothermic transition is observed at ∼120 °C in this case), the de-cross-linking reaction takes place, leading to scission of the DA adduct into its original constitutive moieties (the maleimide group in BMIH and the furan group in EHM-co-FMA). This feature is a first direct evidence of the successful formation of the reversible DA adduct.[48,49] Further proof of the reversibility of the DA adduct was obtained by solubility tests. The solid, thermally treated, coating was immersed in 1,2-dichlorobenzene (DCB), heated to 150 °C, and maintained at that temperature for 2 h under magnetic stirring. The use of DCB was in this case justified by the need of having a good solvent for both BMIH and EHM-co-FMA, while simultaneously having a sufficiently high boiling temperature to avoid evaporation during the test (T_b = 180 °C for DCB). While the coating was shown to be insoluble in DCB at temperatures lower than those characterizing the onset of the endothermic retro-DA transition, higher temperatures (150 °C in this case) led to complete dissolution, clearly suggesting that the retro-DA de-cross-linking reaction had occurred with formation of BMIH and EHM-co-FMA, which are both soluble in DCB (Figure S3). These observations demonstrate the complete reversibility of the chemical bonds formed in the coating upon cross-linking. Similarly, excellent reversibility of the retro-DA/DA process was also observed from DSC analyses conducted on the DA polymer after subjecting it to successive thermal cycles used for the healing process (Figure S4).

The thermo-oxidative response of the cross-linked DA coating was assessed by thermogravimetric analysis (TGA) in air. As shown in Figure 1c, no mass loss events were observed up to 160 °C, above which the coating material exhibited a broad and complex thermodegradation profile involving the complete de-cross-linking of its macromolecular structure. This behavior provides additional proof of the excellent thermal stability of the material also at temperatures compatible with the retro-DA process.

The DA cross-linked coating was also found to display excellent optical clarity, as demonstrated by the high level of transmittance (>90%, comparable with the more commonly used PMMA) over the entire visible spectrum (Figure 1d). Similarly, its refractive index (n_{DA} = 1.54 at 589 nm) is in line with other state-of-the-art acrylate-based systems.[10] These observations further support the suitability of the DA coating for application as an LSC host matrix.

From a functional perspective, selection of the reversible DA reaction was aimed at providing the coating with self-healing capabilities upon application of an external thermal stimulus. The possibility to reversibly control the covalent linkages between EHM-co-FMA and BMIH via the formation/decomposition of the DA adduct represents a powerful tool to repair mechanical damages present on the surface of the DA coating.[50] To assess this self-healing response, the DA coating was mechanically damaged by means of a lancet to produce ∼50 μm wide scratches on its surface. As shown in Figure 1e, after a suitable thermal treatment (150 °C for 20 min, followed by slow cooling to room temperature) complete recovery of the induced surface damage could be achieved with no sign of residual defects on the coating, directly proving the excellent thermal healing ability of this system. It is worth highlighting that the thickness of the coating represents a key parameter for the success of healing processes based on covalent bond rupture and re-formation. In particular, for the damage recovery process to occur effectively, it is essential that the surfaces separated by the cut be in contact during the heat treatment to enable effective formation of the reversible adduct. To this end, the depth of the mechanical damage needs to be less than the coating thickness; otherwise, the groove created by the scratch would reach the underlying substrate, leaving no material to connect the two displaced interfaces and making the damage recovery process impossible. Thus, the coating thickness represents an upper limit for the surface scratch depth to ensure successful healing. In the present case (∼3 μm thick coatings), it was observed that surface scratches as deep as 1.5−2 μm could be healed successfully.

Surface profilometry measurements were conducted after multiple damage/healing cycles to characterize the evolution of the surface morphology and roughness. As shown in Figure S5, no evident changes were observed in the coating morphology after up to four repeat thermal healing cycles. In addition, the values of root-mean-square roughness calculated for the coating after successive damage/healing cycles (see the Supporting Information) confirmed that the surface retained its original features even under repeated thermal stresses.

Given the positive characteristics described above, the suitability of the undoped standard (equimolar) DA coating as a stimulus-responsive host matrix material for LSCs was then investigated following incorporation of a suitable luminescent species, which serves the function of a light-management downshifting center. Because of its favorable chemical−physical and optical properties, the commercially available perylene-based Lumogen F Red 305 (by BASF, here on termed LR305) is ubiquitous as a luminophore in LSCs,[1]
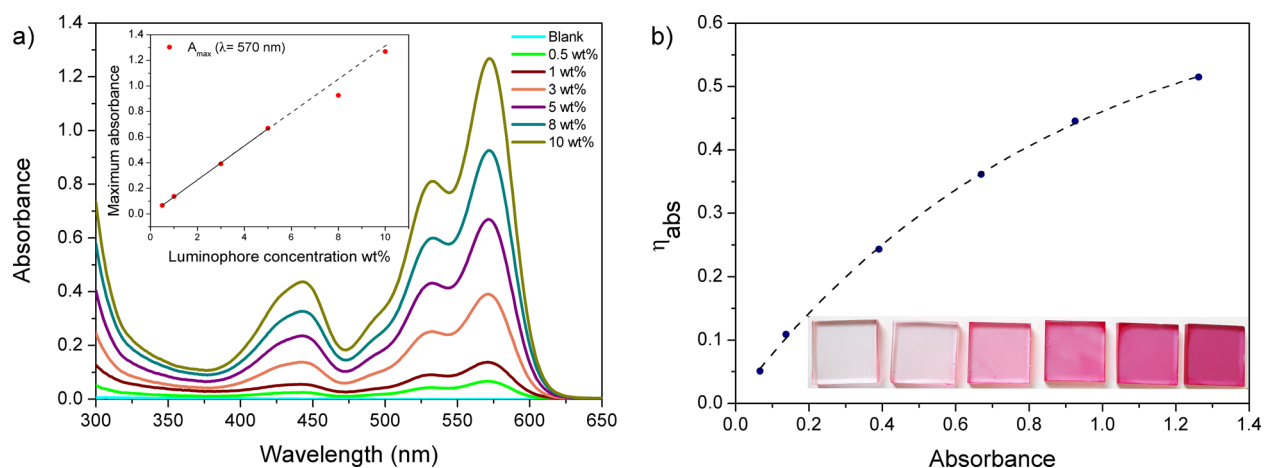
Figure 2. (a) UV/vis absorption spectra of DA-based LSCs at increasing luminophore concentrations. Inset: maximum absorbance vs luminophore concentration (the line indicates the linear fit to the experimental data). (b) Absorption efficiency (η_{abs}) of the LSC system at maximum absorbance (the dashed line represents an exponential fit to the experimental results, and the fitting equation is presented in the main text). Inset: photographic image of DA-based LSCs at increasing luminophore concentrations under natural light.
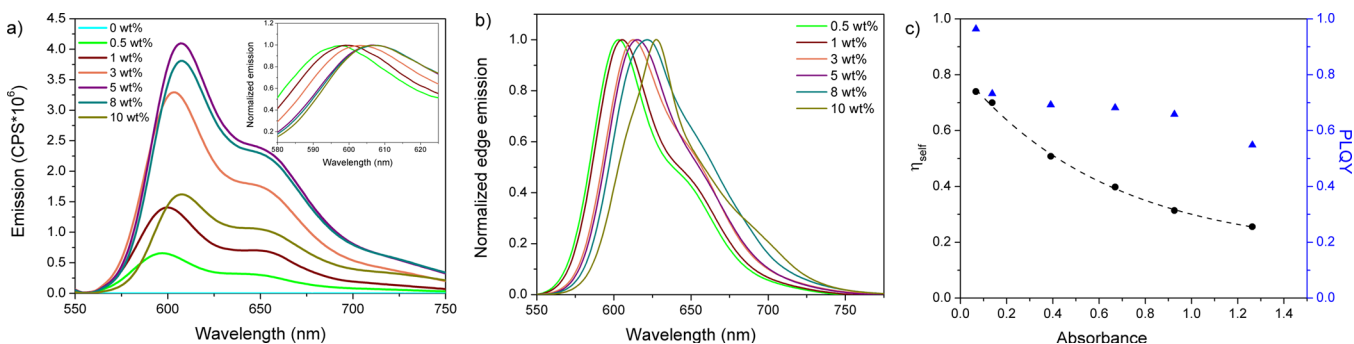

Figure 3. (a) PL spectra of DA-based LSC systems at increasing LR305 concentrations recorded in the front-face-emission configuration. Inset: normalized emission maxima. (b) Normalized PL spectra obtained from edge-emission measurements at increasing luminophore concentrations. (c) Self-absorption efficiency (η_{self}) and PLQY vs absorbance; the exponential fit to η_{self} is also shown (dashed line, fitting equation reported in the main text).

making it a convenient reference platform to evaluate the properties of new host materials. Initially, solubility tests were performed on the luminescent cross-linked coating in THF to examine the presence of any interactions between LR305 and the host and the effect of luminophore incorporation on the self-healing properties of the DA polymer (Figure S6). Complete extraction of LR305 was observed, with no chemical dissolution of the host matrix, clearly demonstrating that no chemical bond forms between LR305 and the DA matrix during cross-linking (host–guest interaction). The gel content of the host matrix (obtained by gravimetric evaluation before and after solvent extraction) was found to be higher than 99%, providing direct evidence of complete cross-linking in the presence of the luminophore. Furthermore, addition of LR305 did not interfere with the functional response of the DA system, as evidenced by the complete recovery of surface damages (Figure S7).

The effect of luminophore concentration on the optical properties was first investigated by UV/vis absorption spectroscopy. As shown in Figure 2a, the characteristic absorption features of LR305 could be clearly distinguished with a linear correlation (Beer–Lambert law) between absorbance and luminophore concentration observed for LR305 loadings up to 5 wt % (see the inset in Figure 2a).

Slight deviations from linearity were found at higher loadings, suggesting reduced solubility of the luminophore in the matrix. The absorption efficiency (η_{abs}) was determined by comparing the overlap of the absorption spectra of the LSCs with the emission spectrum of the incident light source (AM1.5G solar simulator) used for LSC characterization in the 300−650 nm region, i.e., where LR305 absorbs (see the Supporting Information, eq S1, and Figures S8 and S9 for details; calculations for the full solar spectrum also shown). This parameter represents the fraction of incident light that can be effectively absorbed by the LSC, thus providing direct estimation of one of the primary loss modes associated with the nonideal optical properties of the luminophore. As shown in Figure 2b, η_{abs} was found to gradually increase with absorbance following an exponential trend that can be well-fitted by $\eta_{abs} = 0.68 - 0.67 \exp(-1.14 A_{max})$ (A_{max} is the peak absorbance at 570 nm). These trends are in good agreement with values previously reported on reference thin-film LR305/PMMA LSCs.[51]

The photoluminescence (PL) spectra of LR305-doped DA-LSCs were then evaluated. As observed in Figure 3a, in the front-face configuration the emission intensity was found to increase gradually with luminophore concentration up to a threshold concentration of 5−8 wt %. Above this limit, a noticeable decrease in the PL intensity was observed, despite
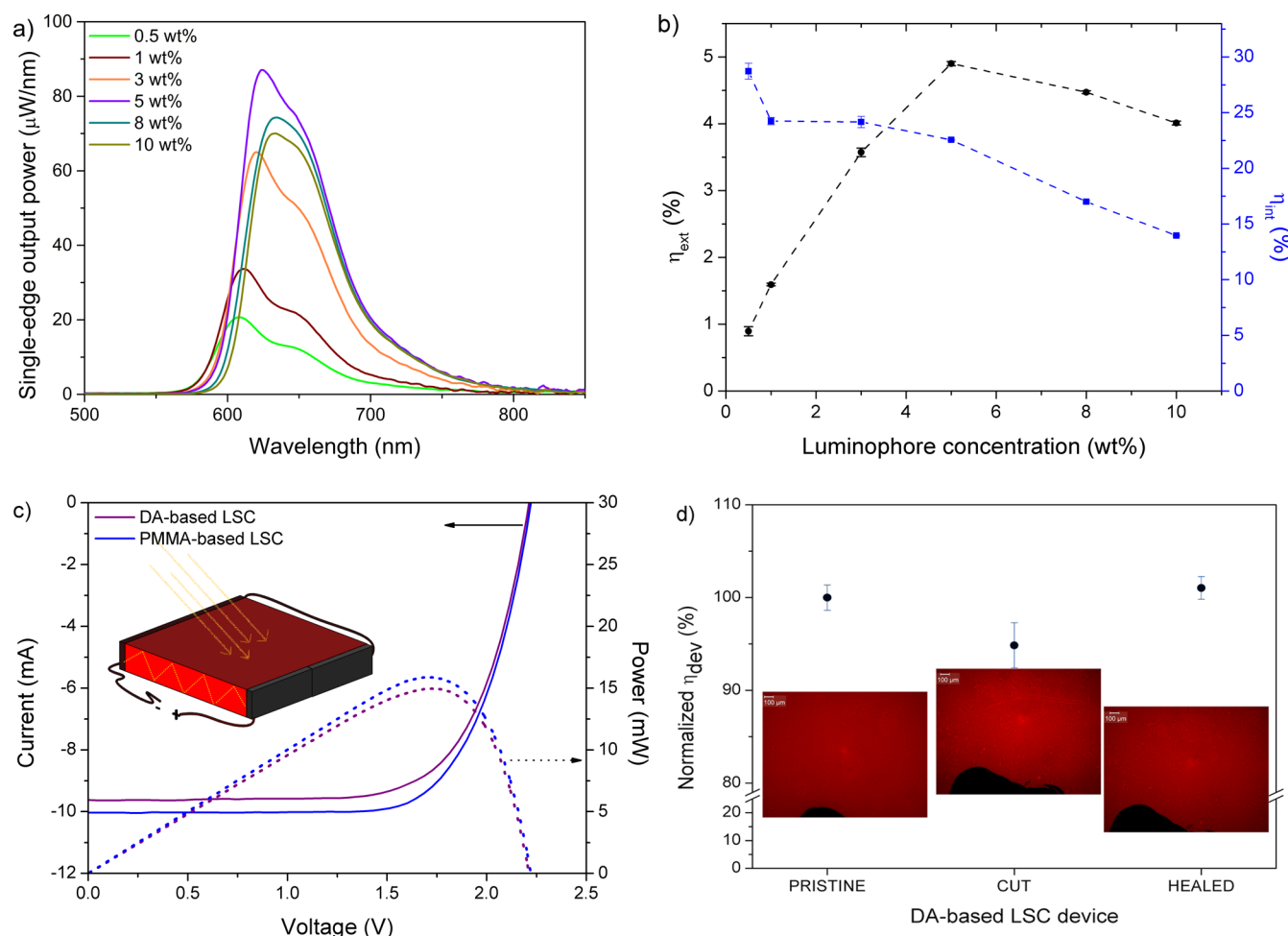
Figure 4. (a) Single-edge optical power spectra of DA-based LSC systems at increasing LR305 concentrations. (b) External photon efficiency η_{ext} and internal photon efficiency η_{int} vs luminophore concentration. (c) $I-V$ curves of optimal DA-based LSC and reference PMMA-based LSC (5 wt % LR305). Inset: schematic representation of the LSC device architecture used in this work. (d) Device efficiency (η_{dev}) of pristine, cut, and healed DA-based LSC.

the steady increase in absorbance (see Figure S10), which was accompanied by a bathochromic shift of the peak maximum (Figure 3a, inset). These trends suggest the presence of dissipative processes in highly concentrated LSCs (>5−8 wt %) causing a portion of the absorbed photons to be lost via nonradiative pathways through reabsorption of emitted photons either due to the small Stokes shift or due to the formation of molecular aggregates through $\pi-\pi$ stacking interactions.[52−55] Detection in the edge-emission configuration (Figure 3b) supports this observation, in which a progressive red-shift of the emission peak is observed with increasing luminophore concentration, as a result of such dissipative phenomena. Loss of vibronic fine structure and broadening of the emission spectrum was also observed. This spectral distortion, not observable in the front-face emission spectra, is a result of the longer optical path traveled by the emitted photons prior to exiting the LSC (edge length vs coating thickness, respectively). Consequently, first-generation emitted photons will have a higher probability of undergoing multiple reabsorption events during the light-guiding process, resulting in the emission of higher generation photons with broader energy distribution. This process will be exacerbated with increasing luminophore concentration due to the decreased distance between adjacent molecules. The self-absorption

efficiency η_{self} was calculated from the recorded edge-emission spectra, scaled to match the true emission spectrum of the luminophore in dilute solution in the long wavelength region (>700 nm) where no self-absorption effects are observed.[23,51] In the absence of self-absorption phenomena, η_{self} will tend to unity (see eq S2 and Figure S11). As shown in Figure 3c, η_{self} was found to decrease for increasing maximum absorbance (A_{max}) values (viz. luminophore concentration) following an exponential decay that could be fitted by $\eta_{self} = 0.16 + 0.65 \exp(-1.56 A_{max})$. Accordingly, a maximum $\eta_{self} = 0.81$ can be predicted for low absorbance (A_{max} tending to zero) where self-absorption is expected to be negligible. On the other hand, in highly concentrated LSCs (high A_{max}) self-absorption effects result in a minimum $\eta_{self} = 0.16$; i.e., a significant fraction of emitted photons (84%) are expected to undergo self-absorption.

As shown in Figure 3c, the PLQY[23,56] approaches unity for very dilute DA-LSCs and maintains a relatively constant value (∼0.7) for intermediate luminophore concentrations (i.e., $A = 0.1-1.0$) before decreasing further (∼0.55) for highly doped LSCs ($A > 1.0$). This trend further confirms the detrimental effect of the formation of nonluminescent aggregates at increasing luminophore concentrations, in which nonradiative decay process become more prevalent.[53,54,57,58] Notably, the

optical characteristics of the LR305-DA-based LSCs are consistent with values previously reported on reference thin-film LSCs in which LR305 was embedded in PMMA,[51] thus indicating that the DA-based matrix proposed here provides the luminophore with a similar environment to that of state-of-the-art polymeric hosts.

The performance of LSCs is typically characterized by the external photon efficiency (η_{ext}), determined experimentally as the ratio between the output photon flux measured at the edges of the LSC (N_{ph-out}) with respect to the incident photon flux (N_{ph-in}). For DA-LSCs with increasing luminophore concentrations, η_{ext} was obtained by illuminating the top face of the LSC with AM1.5G simulated sunlight and by measuring the amount of light exiting the edges of the device using a spectroradiometer connected to an integrating sphere (see Figure S12 and eqs S3 and S4). In this way, the average output-power spectra emitted from the four edges of each LSC in the presence of a dark background could be recorded, with their integration in the 300−800 nm range with respect to N_{ph-in} giving the average values of η_{ext}.[59] As shown in Figure 4a, a red-shift and a change in shape were observed in the output power spectra with increasing LR305 concentration, in good agreement with the edge-emission spectra (Figure 3). The integrated edge-emitted photon flux (four edges) allowed η_{ext} to be calculated, which was found to increase with concentration, reaching a maximum η_{ext} = 4.9% at 5 wt % (Figure 4b). At higher concentrations, η_{ext} was found to decrease in line with the optical loss pathways occurring at high luminophore levels described above (numerical results for edge output power are reported in Table S1). To evaluate the photon transport process within the waveguide, the internal photon efficiency (η_{int}) was calculated from the edge-emitted power spectra as the ratio between N_{ph-out} and the fraction of photons effectively absorbed by the LSC (N_{ph-abs}, obtained by convoluting the absorption spectrum of the DA-based LSC waveguide at increasing luminophore concentration and the incident simulated sunlight spectrum). As shown in Figure 4b, a maximum η_{int} = 28.72% was found for highly dilute systems (LR305 ∼ 0.5 wt %), while in the 1−5 wt % range a relatively constant η_{int} was observed (∼24%), accompanied by a sharp decrease at the highest luminophore loadings (>5 wt %). As expected, this trend agrees well with that observed for the PLQY (Figure 3c).

While direct comparisons with other literature reports are made difficult by the extreme variability encountered in the field when reporting LSC performance parameters and by the strong dependence of the LSC efficiency on measurement conditions and device architecture, it is worth noticing that the maximum η_{ext} values obtained here are in line with other recently reported results found on LSC systems employing LR305 as luminescent species,[23,60] further highlighting the excellent performance of our new DA-based LSC matrix.

To assess the practical viability of our new LSC system, four c-Si PV cells connected in series were edge-coupled to the glass substrate of the LR305-doped DA-based thin-film LSC by using an ethylene−vinyl acetate (EVA) adhesive (Figure 4c). Based on the results obtained from η_{ext} edge-emission measurements (Figure 4), 5 wt % was selected as the optimum LR305 loading. The performance of the assembled LSC-PV system was evaluated under standard illumination conditions (AM 1.5G) by measuring the power conversion efficiency of the resulting LSC device (η_{dev}), defined as the electrical power

effectively extracted from the PV cells (P_{el}^{out}) relative to the luminous power hitting the top surface of the LSC (P_{opt}^{in}):

$$\eta_{dev} = \frac{P_{el}^{out}}{P_{opt}^{in}} = \frac{FF \cdot I_{SC} \cdot V_{OC}}{P_{opt}^{in} \cdot A_{LSC}} \tag{1}$$

where FF, I_{SC}, and V_{OC} are the fill factor, short-circuit current, and open-circuit voltage of the edge-mounted PV cells, respectively, A_{LSC} is the front-illuminated area of the LSC device, and P_{opt}^{in} is the incident solar power density expressed in mW cm^{-2}. A shown in Figure 4c, a maximum I_{SC} of 9.56 mA and a maximum output power of 4.8 mW were achieved, leading to a maximum η_{dev} of 0.79%. It is worth highlighting that these values appear to be among the highest device efficiencies recently reported for LSC thin-film devices in similar testing conditions (namely in the presence of a dark absorbing background and without employing any reflective element at the free edges of the waveguide).[19,61,62] To directly benchmark our system with a reference LSC device, thin-film LSCs based on LR305-doped PMMA were also fabricated onto glass waveguides and coupled with c-Si PV cells. PMMA was selected as reference host matrix due to its wide use in the LSC field.[10,14] The same optical density as the one characterizing our champion devices was used in PMMA-based LSCs (∼0.7), so that appropriate comparisons between the two different systems could be performed reliably. By use of the same device configuration and same testing conditions, the LR305-PMMA LSC exhibited an I_{SC} and a maximum power output of 10.05 mA and 5 mW, respectively, yielding an overall η_{dev} of 0.84%. These results are in line with those obtained on our DA-based LSC, further demonstrating the direct applicability of this novel matrix material as promising component for high-performance thin-film LSCs.

Finally, to investigate the thermally induced healing ability of the DA-based LSC assembly and to assess the effect of surface damages on the output performance of PV-coupled LSCs, tests on mechanically damaged and thermally treated LSCs were carried out. To mimic the presence of scratches potentially forming on the LSC during outdoor service life as a result of physical interactions with solid particles, a lancet was used to induce mechanical damages on the LR305(5 wt %)-DA-based coating. As shown in Figure 4d, after scratching, the luminescent coatings appeared visibly ruined, also to the naked eye. This led to a noticeable (6%) decrease in η_{dev} compared with the pristine system, which may be attributed to the reduction in surface smoothness of the LSC upon scratching, yielding an increased photons scattering during transport due to imperfections and optical defects at the waveguide/air interface. Ultimately, this results in reduced photon trapping at the waveguide edges. In the attempt to recover such damages and the corresponding LSC perform-ance, a thermal treatment was performed on the scratched samples (150 °C for 20 min followed by slow cooling) to induce healing. After this thermal treatment, the surface cuts were found to disappear completely. Interestingly, full recovery of the performance of the LSC device was also achieved, yielding a η_{dev} comparable to the original value obtained on pristine samples. This effect is due to DA click−unclick reactions occurring at the molecular level during the thermal treatment, which are capable of restoring the original surface smoothness of the coating, minimizing photon scattering at the surface and recovering the original device efficiency. As additional proof of the robustness of the DA process, the

reversibility was also tested by performing repeated damage and healing cycles while monitoring the effect on device efficiency. As shown in Figure S14, the LSC device was able to successfully recover its performance after each healing cycle, with no noticeable loss in the absolute efficiency.

CONCLUSIONS

In summary, a novel DA-based polymer coating exhibiting excellent self-healing capabilities has been demonstrated for application as the host matrix in thin-film LSC devices. The DA-based matrix was shown to exhibit excellent transmittance (>90%) over the entire visible spectrum, suitable thermal properties (T_g > 60 °C) and excellent temperature-induced self-healing behavior, which allowed surface scratches to be fully repaired upon a mild thermal treatment. By carefully tuning the concentration of luminophore, we could obtain a maximum external photon efficiency as high as 4.9%, in line with recently reported values found on reference LSC systems with similar optical (absorption/emission) characteristics. In addition, comparably remarkable device efficiencies approaching 0.8% were achieved by coupling the DA-based LSC to edge-mounted c-Si PV cells, this value being among the highest recently reported performances for LSC thin-film devices in similar testing conditions. These results clearly demonstrate the excellent performance of this novel LSC platform, making it a potentially viable alternative to conventional thermoplastic polymers (e.g., PC and PMMA) used as LSC waveguides, while providing the additional benefit of self-healing. The healing capability was demonstrated by evaluating device performance on mechanically scratched LSCs before and after healing treatment. While a noticeable decrease in efficiency was observed when the surface of the doped DA-based waveguide was physically damaged, full recovery of the surface scratches and of device efficiency was achieved after a suitable thermal treatment as a result of the DA functionality embedded in the matrix material.

This work provides the first demonstration of optically clear healable polymeric host matrices for LSCs and paves the way for the design of multifunctional thermoresponsive smart LSC systems with high efficiency and improved physical durability.

ASSOCIATED CONTENT

Ⓢ Supporting Information

The Supporting Information is available free of charge at https://pubs.acs.org/doi/10.1021/acsaem.9b02196.

Experimental section, FTIR spectra of DA-based LSC matrix, characterization of the DA-based host matrix, characterization of luminescent DA-based system, optical characterization of DA-based LSC (PDF)

AUTHOR INFORMATION

Corresponding Author

*E-mail: gianmarco.griffini@polimi.it.

ORCID Ⓘ

Giovanni Fortunato: 0000-0002-8922-8081
Stefano Turri: 0000-0001-8996-0603
Rachel C. Evans: 0000-0003-2956-4857
Gianmarco Griffini: 0000-0002-9924-1722

Author Contributions

E.T., G.F., and B.R. contributed equally to this work.

REFERENCES

(1) Debije, M. G.; Verbunt, P. P. C. Thirty Years of Luminescent Solar Concentrator Research: Solar Energy for the Built Environment. *Adv. Energy Mater.* **2012**, *2*, 12−35.

(2) Meinardi, F.; Bruni, F.; Brovelli, S. Luminescent Solar Concentrators for Building-Integrated Photovoltaics. *Nat. Rev. Mater.* **2017**, *2*, 1−9.

(3) Traverse, C. J.; Pandey, R.; Barr, M. C.; Lunt, R. R. Emergence of Highly Transparent Photovoltaics for Distributed Applications. *Nat. Energy* **2017**, *2*, 849−860.

(4) Mckenna, B.; Evans, R. C. Towards Efficient Spectral Converters through Materials Design for Luminescent Solar Devices. *Adv. Mater.* **2017**, *29*, 1606491.

(5) Pucci, A. Luminescent Solar Concentrators Based on Aggregation Induced Emission. *Isr. J. Chem.* **2018**, *58*, 837−844.

(6) Moraitis, P.; Schropp, R. E. I.; van Sark, W. G. J. H. M. Nanoparticles for Luminescent Solar Concentrators - A Review. *Opt. Mater. (Amsterdam, Neth.)* **2018**, *84*, 636−645.

(7) Zhou, Y.; Zhao, H.; Ma, D.; Rosei, F. Harnessing the Properties of Colloidal Quantum Dots in Luminescent Solar Concentrators. *Chem. Soc. Rev.* **2018**, *47*, 5866−5890.

(8) Griffini, G.; Brambilla, L.; Levi, M.; Castiglioni, C.; Del Zoppo, M.; Turri, S. Anthracene/Tetracene Cocrystals as Novel Fluorophores in Thin-Film Luminescent Solar Concentrators. *RSC Adv.* **2014**, *4*, 9893−9897.

(9) Mazzaro, R.; Vomiero, A. The Renaissance of Luminescent Solar Concentrators: The Role of Inorganic Nanomaterials. *Adv. Energy Mater.* **2018**, *8*, 1801903.

(10) Zettl, M.; Mayer, O.; Klampaftis, E.; Richards, B. S. Investigation of Host Polymers for Luminescent Solar Concentrators. *Energy Technol.* **2017**, *5*, 1037−1044.

(11) Reisfeld, R.; Shamrakov, D.; Jorgensen, C. Photostable Solar Concentrators Based on Fluorescent Glass Films. *Sol. Energy Mater. Sol. Cells* **1994**, *33*, 417−427.

(12) Desmet, L.; Ras, A. J. M.; de Boer, D. K. G.; Debije, M. G. Monocrystalline Silicon Photovoltaic Luminescent Solar Concentrator with 42% Power Conversion Efficiency. *Opt. Lett.* **2012**, *37*, 3087.

(13) Hinsch, A.; Zastrow, A.; Wittwer, V. Sol-Gel Glasses: A New Material for Solar Fluorescent Planar Concentrators? *Sol. Energy Mater.* **1990**, *21*, 151−164.

(14) Griffini, G. Host Matrix Materials for Luminescent Solar Concentrators: Recent Achievements and Forthcoming Challenges. *Front. Mater.* **2019**, *6*, 1−8.

(15) Fattori, V.; Melucci, M.; Ferrante, L.; Zambianchi, M.; Manet, I.; Oberhauser, W.; Giambastiani, G.; Frediani, M.; Giachi, G.; Camaioni, N. Poly(Lactic Acid) as a Transparent Matrix for Luminescent Solar Concentrators: A Renewable Material for a Renewable Energy Technology. *Energy Environ. Sci.* **2011**, *4*, 2849−2853.

(16) Melucci, M.; Durso, M.; Favaretto, L.; Capobianco, M. L.; Benfenati, V.; Sagnella, A.; Ruani, G.; Muccini, M.; Zamboni, R.; Fattori, V.; Camaioni, N. Silk Doped with a Bio-Modified Dye as a Viable Platform for Eco-Friendly Luminescent Solar Concentrators. *RSC Adv.* **2012**, *2*, 8610−8613.

(17) Geervliet, T. A.; Gavrila, I.; Iasilli, G.; Picchioni, F.; Pucci, A. Luminescent Solar Concentrators Based on Renewable Polyester Matrices. *Chem. - Asian J.* **2019**, *14*, 877−883.

(18) Maggioni, G.; Campagnaro, A.; Carturan, S.; Quaranta, A. Dye-Doped Parylene-Based Thin Film Materials: Application to Luminescent Solar Concentrators. *Sol. Energy Mater. Sol. Cells* **2013**, *108*, 27−37.

(19) Tonezzer, M.; Maggioni, G.; Campagnaro, A.; Carturan, S.; Quaranta, A.; della Pirriera, M.; Gutierrez Tauste, D. Luminescent Solar Concentrators Employing New Eu(TTA)3phen-Containing Parylene Films. *Prog. Photovoltaics* **2015**, *23*, 1037−1044.

(20) Credi, C.; Pintossi, D.; Bianchi, C. L.; Levi, M.; Griffini, G.; Turri, S. Combining Stereolithography and Replica Molding: On the Way to Superhydrophobic Polymeric Devices for Photovoltaics. *Mater. Des.* **2017**, *133*, 143−153.

(21) Griffini, G.; Levi, M.; Turri, S. Novel Crosslinked Host Matrices Based on Fluorinated Polymers for Long-Term Durability in Thin-Film Luminescent Solar Concentrators. *Sol. Energy Mater. Sol. Cells* **2013**, *118*, 36−42.

(22) Griffini, G.; Levi, M.; Turri, S. Novel High-Durability Luminescent Solar Concentrators Based on Fluoropolymer Coatings. *Prog. Org. Coat.* **2014**, *77*, 528−536.

(23) Kaniyoor, A.; Mckenna, B.; Comby, S.; Evans, R. C. Design and Response of High-Efficiency, Planar, Doped Luminescent Solar Concentrators Using Organic-Inorganic Di-Ureasil Waveguides. *Adv. Opt. Mater.* **2016**, *4*, 444−456.

(24) Rondão, R.; Frias, A. R.; Correia, S. F. H.; Fu, L.; De Zea Bermudez, V.; André, P. S.; Ferreira, R. A. S.; Carlos, L. D. High-Performance Near-Infrared Luminescent Solar Concentrators. *ACS Appl. Mater. Interfaces* **2017**, *9*, 12540−12546.

(25) Nolasco, M. M.; Vaz, P. M.; Freitas, V. T.; Lima, P. P.; André, P. S.; Ferreira, R. A. S.; Vaz, P. D.; Ribeiro-Claro, P.; Carlos, L. D. Engineering Highly Efficient Eu(Iii)-Based Tri-Ureasil Hybrids toward Luminescent Solar Concentrators. *J. Mater. Chem. A* **2013**, *1*, 7339−7350.

(26) Frias, A. R.; Pecoraro, E.; Correia, S. F. H.; Minas, L. M. G.; Bastos, A. R.; García-Revilla, S.; Balda, R.; Ribeiro, S. J. L.; André, P. S.; Carlos, L. D.; Ferreira, R. A. S. Sustainable Luminescent Solar Concentrators Based on Organic-Inorganic Hybrids Modified with Chlorophyll. *J. Mater. Chem. A* **2018**, *6*, 8712−8723.

(27) Correia, S. F. H.; Lima, P. P.; Pecoraro, E.; Ribeiro, S. J. L.; André, P. S.; Ferreira, R. A. S.; Carlos, L. D. Scale up the Collection Area of Luminescent Solar Concentrators towards Metre-Length Flexible Waveguiding Photovoltaics. *Prog. Photovoltaics* **2016**, *24*, 1178−1193.

(28) Correia, S. F. H.; Lima, P. P.; André, P. S.; Ferreira, M. R. S.; Carlos, L. D. High-Efficiency Luminescent Solar Concentrators for Flexible Waveguiding Photovoltaics. *Sol. Energy Mater. Sol. Cells* **2015**, *138*, 51−57.

(29) Wu, K.; Li, H.; Klimov, V. I. Tandem Luminescent Solar Concentrators Based on Engineered Quantum Dots. *Nat. Photonics* **2018**, *12*, 105−110.

(30) Xu, L.; Yao, Y.; Bronstein, N. D.; Li, L.; Alivisatos, A. P.; Nuzzo, R. G. Enhanced Photon Collection in Luminescent Solar Concentrators with Distributed Bragg Reflectors. *ACS Photonics* **2016**, *3*, 278−285.

(31) Yoon, J.; Li, L.; Semichaevsky, A. V.; Ryu, J. H.; Johnson, H. T.; Nuzzo, R. G.; Rogers, J. A. Flexible Concentrator Photovoltaics Based on Microscale Silicon Solar Cells Embedded in Luminescent Waveguides. *Nat. Commun.* **2011**, *2*, 343−348.

(32) Sol, J. A. H. P.; Dehm, V.; Hecht, R.; Würthner, F.; Schenning, A. P. H. J.; Debije, M. G. Temperature-Responsive Luminescent Solar Concentrators: Tuning Energy Transfer in a Liquid Crystalline Matrix. *Angew. Chem., Int. Ed.* **2018**, *57*, 1030−1033.

(33) Pintossi, D.; Colombo, A.; Levi, M.; Dragonetti, C.; Turri, S.; Griffini, G. UV-Curable Fluoropolymers Crosslinked with Functional Fluorescent Dyes: The Way to Multifunctional Thin-Film Luminescent Solar Concentrators. *J. Mater. Chem. A* **2017**, *5*, 9067−9075.

(34) Meazzini, I.; Blayo, C.; Arlt, J.; Marques, A. T.; Scherf, U.; Burrows, H. D.; Evans, R. C. Ureasil Organic-Inorganic Hybrids as Photoactive Waveguides for Conjugated Polyelectrolyte Luminescent Solar Concentrators. *Mater. Chem. Front.* **2017**, *1*, 2271−2282.

(35) Mulder, C. L.; Reusswig, P. D.; Beyler, A. P.; Kim, H.; Rotschild, C.; Baldo, M. A. Dye Alignment in Luminescent Solar Concentrators: II Horizontal Alignment for Energy Harvesting in Linear Polarizers. *Opt. Express* **2010**, *18*, A91−A99.

(36) Mulder, C. L.; Reusswig, P. D.; Velázquez, A. M.; Kim, H.; Rotschild, C.; Baldo, M. A. Dye Alignment in Luminescent Solar Concentrators: I Vertical Alignment for Improved Waveguide Coupling. *Opt. Express* **2010**, *18*, A79−A90.

(37) Banal, J. L.; Zhang, B.; Jones, D. J.; Ghiggino, K. P.; Wong, W. W. H. Emissive Molecular Aggregates and Energy Migration in Luminescent Solar Concentrators. *Acc. Chem. Res.* **2017**, *50*, 49−57.

(38) Slooff, L. H.; Bende, E. E.; Burgers, A. R.; Budel, T.; Pravettoni, M.; Kenny, R. P.; Dunlop, E. D.; Büchtemann, A. A Luminescent Solar Concentrator with 7.1% Power Conversion Efficiency. *Phys. Status Solidi RRL* **2008**, *2*, 257−259.

(39) Currie, M. J.; Mapel, J. K.; Heidel, T. D.; Goffri, S.; Baldo, M. A. High-Efficiency Organic Solar Concentrators for Photovoltaics. *Science* **2008**, *321*, 226−228.

(40) Griffini, G.; Brambilla, L.; Levi, M.; Del Zoppo, M.; Turri, S. Photo-Degradation of a Perylene-Based Organic Luminescent Solar Concentrator: Molecular Aspects and Device Implications. *Sol. Energy Mater. Sol. Cells* **2013**, *111*, 41−48.

(41) Batchelder, J. S.; Zewail, A. H.; Cole, T. Wren Rosenzweig 1991 Habitat Selection.pdf, 1979; p 18.

(42) Batchelder, J. S.; Zewail, A. H.; Cole, T. Luminescent Solar Concentrators 2: Experimental and Theoretical Analysis of Their Possible Efficiencies. *Appl. Opt.* **1981**, *20*, 3733.

(43) Tummeltshammer, C.; Taylor, A.; Kenyon, A. J.; Papakonstantinou, I. Losses in Luminescent Solar Concentrators Unveiled. *Sol. Energy Mater. Sol. Cells* **2016**, *144*, 40−47.

(44) Thomas, W. R. L.; Drake, J. M.; Lesiecki, M. L. Light Transport in Planar Luminescent Solar Concentrators: The Role of Matrix Losses. *Appl. Opt.* **1983**, *22*, 3440.

(45) Gandini, A. The Furan/Maleimide Diels-Alder Reaction: A Versatile Click-Unclick Tool in Macromolecular Synthesis. *Prog. Polym. Sci.* **2013**, *38*, 1−29.

(46) Laita, H.; Boufi, S.; Gandini, A. The Application of the Diels-Alder Reaction to Polymers Bearing Furan Moieties. 1. Reactions with Maleimides. *Eur. Polym. J.* **1997**, *33*, 1203−1211.

(47) Alonso García, M. C.; Balenzategui, J. L. Estimation of Photovoltaic Module Yearly Temperature and Performance Based on Nominal Operation Cell Temperature Calculations. *Renewable Energy* **2004**, *29*, 1997−2010.

(48) Froidevaux, V.; Borne, M.; Laborbe, E.; Auvergne, R.; Gandini, A.; Boutevin, B. Study of the Diels-Alder and Retro-Diels-Alder Reaction between Furan Derivatives and Maleimide for the Creation of New Materials. *RSC Adv.* **2015**, *5*, 37742−37754.

(49) Boutelle, R. C.; Northrop, B. H. Substituent Effects on the Reversibility of Furan - Maleimide Cycloadditions. *J. Org. Chem.* **2011**, *76*, 7994−8002.

(50) Liu, Y. L.; Chuo, T. W. Self-Healing Polymers Based on Thermally Reversible Diels-Alder Chemistry. *Polym. Chem.* **2013**, *4*, 2194−2205.

(51) Dienel, T.; Bauer, C.; Dolamic, I.; Bruhwiler, D. Spectral-Based Analysis of Thin Film Luminescent Solar Concentrators. *Sol. Energy* **2010**, *84*, 1366−1369.

(52) Griffini, G.; Levi, M.; Turri, S. Thin-Film Luminescent Solar Concentrators: A Device Study towards Rational Design. *Renewable Energy* **2015**, *78*, 288−294.

(53) Yoo, H.; Yang, J.; Yousef, A.; Wasielewski, M. R.; Kim, D. Excimer Formation Dynamics of Intramolecular π-Stacked Perylene-diimides Probed by Single-Molecule Fluorescence Spectroscopy. *J. Am. Chem. Soc.* **2010**, *132*, 3939−3944.

(54) Haines, C.; Chen, M.; Ghiggino, K. P. The Effect of Perylene Diimide Aggregation on the Light Collection Efficiency of Luminescent Concentrators. *Sol. Energy Mater. Sol. Cells* **2012**, *105*, 287−292.

(55) Al-Kaysi, R. O.; Sang Ahn, T.; Müller, A. M.; Bardeen, C. J. The Photophysical Properties of Chromophores at High (100 MM and

above) Concentrations in Polymers and as Neat Solids. *Phys. Chem. Chem. Phys.* **2006**, *8*, 3453−3459.

(56) De Mello, J. C.; Wittmann, H. F.; Friend, R. H. An Improved Experimental Determination of External Photoluminescence Quantum Efficiency. *Adv. Mater.* **1997**, *9*, 230−232.

(57) Buffa, M.; Debije, M. G. Dye-Doped Polysiloxane Rubbers for Luminescent Solar Concentrator Systems. *Springer Ser. Mater. Sci.* **2014**, *190*, 247−266.

(58) Wilson, L. R.; Rowan, B. C.; Robertson, N.; Moudam, O.; Jones, A. C.; Richards, B. S. Characterization and Reduction of Reabsorption Losses in Luminescent Solar Concentrators. *Appl. Opt.* **2010**, *49*, 1651.

(59) Debije, M. G.; Teunissen, J. P.; Kastelijn, M. J.; Verbunt, P. P. C.; Bastiaansen, C. W. M. The Effect of a Scattering Layer on the Edge Output of a Luminescent Solar Concentrator. *Sol. Energy Mater. Sol. Cells* **2009**, *93*, 1345−1350.

(60) Albers, P. T. M.; Bastiaansen, C. W. M.; Debije, M. G. Dual Waveguide Patterned Luminescent Solar Concentrators. *Sol. Energy* **2013**, *95*, 216−223.

(61) Zhao, Y.; Lunt, R. R. Transparent Luminescent Solar Concentrators for Large-Area Solar Windows Enabled by Massive Stokes-Shift Nanocluster Phosphors. *Adv. Energy Mater.* **2013**, *3*, 1143−1148.

(62) Banal, J. L.; White, J. M.; Lam, T. W.; Blakers, A. W.; Ghiggino, K. P.; Wong, W. W. H. A Transparent Planar Concentrator Using Aggregates of Gem-Pyrene Ethenes. *Adv. Energy Mater.* **2015**, *5*, 1500818.